Transient absorption and reshaping of ultrafast XUV light by laser-dressed helium

Mette B. Gaarde,[1,2,*] Christian Buth,[1,2,3,†] Jennifer L. Tate,[1] and Kenneth J. Schafer[1,2]

[1]*Department of Physics and Astronomy, Louisiana State University, Baton Rouge, Louisiana 70803, USA*

[2]*The PULSE Institute for Ultrafast Energy Science, SLAC National Accelerator Laboratory, Menlo Park, California 94025, USA*

[3]*Max-Planck-Institut für Kernphysik, Saupfercheckweg 1, 69117 Heidelberg, Germany*

(Received 20 October 2010; published 31 January 2011)

We present a theoretical study of transient absorption and reshaping of extreme ultraviolet (XUV) pulses by helium atoms dressed with a moderately strong infrared (IR) laser field. We formulate the atomic response using both the frequency-dependent absorption cross section and a time-frequency approach based on the time-dependent dipole induced by the light fields. The latter approach can be used in cases when an ultrafast dressing pulse induces transient effects, and/or when the atom exchanges energy with multiple frequency components of the XUV field. We first characterize the dressed atom response by calculating the frequency-dependent absorption cross section for XUV energies between 20 and 24 eV for several dressing wavelengths between 400 and 2000 nm and intensities up to 10^{12} W/cm^2. We find that for dressing wavelengths near 1600 nm, there is an Autler-Townes splitting of the $1s \rightarrow 2p$ transition that can potentially lead to transparency for absorption of XUV light tuned to this transition. We study the effect of this XUV transparency in a macroscopic helium gas by incorporating the time-frequency approach into a solution of the coupled Maxwell-Schrödinger equations. We find rich temporal reshaping dynamics when a 61-fs XUV pulse resonant with the $1s \rightarrow 2p$ transition propagates through a helium gas dressed by an 11-fs, 1600-nm laser pulse.

DOI: 10.1103/PhysRevA.83.013419 PACS number(s): 32.80.Fb, 32.80.Qk, 32.80.Rm, 42.50.Hz

I. INTRODUCTION

The advent of ultrafast XUV and even x-ray light sources that can be synchronized to optical or IR laser pulses has given rise to several recent studies of the transient absorption of such radiation by laser-dressed atoms, both experimental [1–5] and theoretical [6–8]. For example, many of the experiments done in attosecond physics involve the transient absorption of attosecond XUV radiation by atoms interacting with an IR laser field. This is because the strong-field process of high harmonic generation (HHG), which is used to produce the attosecond XUV radiation as either single pulses or trains of pulses, results in the XUV field being precisely synchronized with the driving IR field [1,9]. It is then possible to perform experiments using the XUV field and a replica of the original IR field with attosecond precision [10]. Glover *et al.* also showed that it is possible to overlap pulses of synchrotron-produced soft-x-ray radiation with an 800-nm dressing laser in a study of laser-induced transparency in neon [2].

In this paper we explore how an ultrafast XUV pulse interacts with a simple atom, helium, in the presence of a moderately strong IR field that may be either shorter or longer in duration than the XUV pulse. We have as our goal to formulate theoretical methods that can be used to calculate the absorption and emission of XUV radiation by strongly dressed atoms even when the XUV pulses are on the femtosecond time scale, and may include multiple frequencies in a comb. In addition, we want to be able to study the transient absorption and reshaping of radiation as it propagates through a macroscopic amount of gas. We will restrict ourselves in this study to cases where the IR laser dresses the atom without appreciably exciting it, leaving higher IR intensities for a future paper. We will also restrict ourselves to XUV wavelengths and intensities where single excitations below the first ionization threshold at 24.6 eV dominate the XUV absorption. Even given these restrictions, the IR laser has a substantial impact on the Rydberg and continuum states of the atom and, in this way, enables profound control over resonant XUV absorption [7,11–14].

In the calculations we present we will consider the simplest case, where there are just two radiation fields, one that dresses the atom and one that is absorbed and possibly reshaped. The fundamental problem of a two-color field such as this has been studied before in the context of x-ray absorption by neon [2,7,15–17], argon [18], and krypton [19] atoms. Specifically, the examination of laser-dressed atoms led to the discovery of electromagnetically induced transparency (EIT) for x rays [7], better characterized as Autler-Townes splitting [12] because the transparency is not predominantly caused by destructive interference. Also, there have been several studies of helium in the context of the two-color problem we are discussing. It was investigated with an optical laser and the XUV free-electron laser in Hamburg [20–22], and the impact of laser-dressing helium on the production of XUV radiation via HHG was studied theoretically in Ref. [23].

We begin by characterizing the single-atom response in terms of the cross section for absorption of XUV radiation of frequency ω_X. First we calculate the linear, frequency-dependent XUV absorption cross section using a Floquet-like method [non-Hermitian perturbation theory (NHPT)] that treats the XUV field as a monochromatic source. This method has been extensively tested in the context of x-ray absorption on the $1s \rightarrow 3p$ resonance of laser-dressed neon, alluded to above [7,19]. Next, we outline a method using direct integration of the time-dependent Schrödinger equation (TDSE), which achieves essentially the same goal by using pulses of finite duration. The cross section is extracted by projecting out the initial state from the final-state wave function. The

*gaarde@phys.lsu.edu

†christian.buth@web.de

two methods, NHPT and the TDSE-projection method, are shown to agree when the XUV pulse bandwidth is very small. The TDSE-projection approach is, however, potentially more flexible in dealing with situations where the dressing laser couples many states of the atom. We find that the TDSE-projection method can be used with a reasonable amount of effort to study laser-dressed absorption over a wide range of XUV frequencies and dressing wavelengths. As an example of the usefulness of the method, we show representative results for several dressing wavelengths between 0.4 and 2.0 μm.

Next we extend the treatment of the XUV interaction to deal with cases where the atomic response varies as a function of time or frequency in a nontrivial way. This could, for instance, be because the IR dressing pulse is so short that nonadiabatic effects cause the cross section to vary substantially over the bandwidth of the pulse. Another interesting situation is when the IR pulse is so strong that multiphoton processes cause the atom to exchange energy with the light field over a large range of frequencies in many different orders of nonlinearity, so that it is no longer practical to (artificially) separate the linear (nonlinear) absorption from the driven linear (nonlinear) emission. We therefore develop a time-frequency approach to the atomic response, based on the time-dependent energy exchange between the atom and the light fields. Our method is similar in spirit to the treatment provided by, for instance, Tannor [24] and Pollard and Mathies [25], with the important difference that we are not separating the atomic response into different linear and nonlinear orders but we are keeping everything in one frequency-dependent response function. We find that when we use long (∼30 fs) XUV pulses we get good agreement between linear absorption cross sections calculated using the time-frequency and the TDSE-projection cross section. Having obtained this good agreement over a range of frequencies and dressing laser intensities gives us confidence that we can calculate the full time-frequency response of the dressed atom.

Finally we show how this time-frequency approach is consistent with our solution of the coupled Maxwell wave equation (MWE) and the TDSE. This allows for a generalized, *ab initio* description of linear and nonlinear absorption, emission, and phase matching in a macroscopic medium. We apply this formalism to studying the propagation of an XUV pulse in a macroscopic helium gas dressed by a moderately intense 11-fs, 1600-nm laser pulse. We find that the XUV pulse, which is resonant with the $1s \rightarrow 2p$ transition in the undressed atom, undergoes rich temporal absorption and reshaping dynamics.

The paper is structured as follows. In Sec. II, we first discuss the three formalisms for calculating absorption cross sections of laser-dressed atoms. In Sec. III we present our framework for the macroscopic calculations. Then we use the methods to study laser-dressed helium; computational details are given in Sec. IV and results are presented in Sec. V. We end the paper with a brief conclusion in Sec. VI.

II. SINGLE-ATOM RESPONSE

This section contains three derivations of the one-photon absorption cross section for XUV light interacting with an atom in the presence of a long-wavelength dressing field. All three formalisms are based on the single-active-electron (SAE) approximation, and in all cases we use linearly polarized fields where the IR and XUV polarization vectors are parallel. We use atomic units throughout this section [26].

A. Non-Hermitian Rayleigh-Schrödinger perturbation theory

Our NHPT treatment of dressed XUV absorption is discussed in detail in Refs. [18,19,27]. Here we provide a brief account to highlight the essential steps in the derivation and to facilitate a discussion of the other two formalisms.

In the NHPT formalism, the one-photon XUV absorption cross section follows from

$$\sigma = 2\,\frac{\Gamma_I}{J_X}, \tag{1}$$

where J_X is the constant XUV photon flux of a continuous-wave XUV light source [19], and Γ_I is the transition rate from the initial state to Rydberg orbitals or the continuum. The factor of 2 accounts for the number of electrons in the atomic orbital, which is used as the initial state $|\mathrm{I}\rangle$.

To determine Γ_I with NHPT, the full Hamiltonian of an atom in two-color light $\hat{H} = \hat{H}_0 + \hat{H}_1$ is decomposed into a strongly interacting part $\hat{H}_0 = \hat{H}_{AT} + \hat{H}_{EM,L} + \hat{H}_{I,L} + \hat{H}_{EM,X}$ that contains the atomic electronic structure $\hat{H}_{AT}$ in a Hartree-Fock-Slater approximation [28,29]. The interaction with light is expressed in terms of nonrelativistic quantum electrodynamics [18,19,27]; the free IR laser and XUV fields are $\hat{H}_{EM,L}$ and $\hat{H}_{EM,X}$, respectively, and the interaction of the atomic electrons with the laser field is $\hat{H}_{I,L}$. The weak interaction with the XUV light is represented by $\hat{H}_1 = \hat{H}_{I,X}$ [19].

Next we represent $\hat{H}_0$ in a complex-symmetric direct-product basis of electronic states—without the initial state $|\mathrm{I}\rangle$—and photonic number states. In doing so, we assume that the initial state and its energy E_I are not noticeably influenced by the laser dressing. The matrix representation of $\hat{H}_0$,

$$\boldsymbol{H}_0^{(m)}\vec{c}_F^{\,(m)} = E_F^{(m)}\vec{c}_F^{\,(m)}, \tag{2}$$

is diagonalized, yielding eigenvectors $\vec{c}_F^{\,(m)}$ that represent the expansion coefficients of new laser-dressed states $|F^{(m)}\rangle$ for eigenvalues $E_F^{(m)}$ [19]. Here, m is the magnetic quantum number that is conserved for linearly polarized light.

When the Hamiltonian $\hat{H}_0$ is represented in the new basis of laser-dressed states [Eq. (2)], the excitation or ionization of a ground-state electron of an atom owing to XUV photoabsorption is described as a resonance in the spectrum of the non-Hermitian, complex-symmetric representation of the Hamiltonian in the basis $\{|\mathrm{I}\rangle, |F^{(m)}\rangle | \forall\, F,m\}$ [30–32]. The complex energy of the resonance state that $|\mathrm{I}\rangle$ becomes owing to the coupling to excited states and the continuum via XUV light is usually referred to as the Siegert energy [30,33] and satisfies

$$E_{\mathrm{res}} = E_{\mathrm{R}} - \mathrm{i}\,\Gamma_I/2\,. \tag{3}$$

The real part of the resonance energy is E_R, and Γ_I stands for the transition rate from the ground state to a laser-dressed Rydberg orbital or the laser-dressed continuum [Eq. (2)] via photoabsorption. We determine the Siegert energy [Eq. (3)] of

the initial state $|\mathrm{I}\rangle$ in second-order NHPT. The total transition rate out of $|\mathrm{I}\rangle$ is given by

$$\Gamma_I = 2\,\mathrm{Im}\left[\sum_{m,F}\frac{\langle \mathrm{I}|\hat{H}_1|F^{(m)}\rangle\langle F^{(m)}|\hat{H}_1|\mathrm{I}\rangle}{E_F^{(m)}-E_I}\right], \tag{4}$$

and the absorption cross section is finally obtained from Eqs. (4) and (1) as

$$\sigma(\omega_\mathrm{X}) = 8\pi\alpha\omega_\mathrm{X}\,\mathrm{Im}\left\{\sum_{m,F}\frac{\left[\mathcal{D}_F^{(m)}\right]^2}{E_F^{(m)}-E_I-\omega_\mathrm{X}}\right\}. \tag{5}$$

Here α denotes the fine-structure constant and $\mathcal{D}_F^{(m)}$ is a complex-scaled transition dipole matrix element between the initial state $|\mathrm{I}\rangle$ and the Fth laser-dressed atomic state with projection quantum number m [19].

B. Projection treatment of XUV absorption

As an alternative to the treatment above, we can obtain the linear absorption cross section by a direct solution of the TDSE in the SAE approximation [34]. The cross section is extracted by projecting the final-state wave function obtained at the end of a finite pulse onto the initial wave function. As such, we avoid calculating the dressed states directly, making explicit use of only the laser-free initial and final states.

To simplify the treatment of finite duration pulses when using the projection method, we replace the quantum electrodynamic treatment of XUV radiation in Sec. II A by a semiclassical description of light [35]. We begin by choosing the vector potential of the XUV light of carrier frequency ω_X to be

$$\vec{\mathcal{A}}_X(t) = -\frac{\mathcal{E}_X(t)}{\omega_X}\sin(\omega_X t)\,\vec{e}_x. \tag{6}$$

The electric field of the XUV light field is then given by the derivative with respect to time, $\vec{\mathcal{E}}_X(t) = -\partial\vec{\mathcal{A}}_X(t)/\partial t$:

$$\vec{\mathcal{E}}_X(t) = \left[\mathcal{E}_X(t)\cos(\omega_X t) + \frac{1}{\omega_X}\frac{\partial\mathcal{E}_X(t)}{\partial t}\sin(\omega_X t)\right]\vec{e}_x. \tag{7}$$

Here, $\mathcal{E}_X(t) = \sqrt{8\pi\alpha I_X(t)}$ is the envelope of the XUV pulse and $I_X(t)$ is its cycle-averaged intensity. Our specification of the vector potential in Eq. (6) ensures that the integrated electric field and the vector potential at the end of the pulse, $\mathcal{A}(t_f)$, are zero when $\mathcal{E}_X(t)$ is zero at the initial and final times. It leads to the second term on the right-hand side of Eq. (7), which is a small correction of order $\Delta\omega_X/\omega_X$ near the center of the pulse, for pulses with a bandwidth of $\Delta\omega_X$. By ensuring that $\mathcal{A}(t_f) = 0$, we obtain results that are independent of the electromagnetic gauge.

For a Gaussian envelope pulse with a full width at half maximum (FWHM) duration of τ_X, the bandwidth of the pulse is given by $\Delta\omega_X = 4\ln 2/\tau_X$. In our calculations, we first specify $\Delta\omega_X$ and this dictates the value of τ_X. The Gaussian envelope is then approximated by a trigonometric pulse [36]:

$$I_X(t) = I_{X,0}\cos^{2n}\left(\frac{\pi t}{T_n}\right)\theta\left(\frac{T_n}{2}-|t|\right) \equiv I_{X,0}g_n(t), \tag{8}$$

with an integer $n > 0$ and the Heaviside θ function [37]. The total pulse duration is defined as

$$T_n = \frac{\pi\tau_X}{2\arccos 2^{-\frac{1}{2n}}}, \tag{9}$$

The envelope (8) converges rapidly to a Gaussian function in the limit $\lim_{n\to\infty} g_n(t) \to \exp[-4\ln 2(\frac{t}{\tau_X})^2]$. Using the approximative function (8) instead of a true Gaussian function has the advantage that it goes to zero on a finite support, which allows us to satisfy the requirement $\mathcal{A}(t_f) = 0$ exactly.

In the TDSE-projection formalism we also need to dress the atom with a laser field with frequency ω_L. We do this by using a laser field of the form

$$\vec{\mathcal{E}}_L(t) = \mathcal{E}_L(t)\sin(\omega_L t)\,\vec{e}_L. \tag{10}$$

The envelope function $\mathcal{E}_L(t)$ is now a trapezoidal pulse with a linear ramp of one optical cycle at each end and a flat section that completely spans over the XUV pulse. The pulse contains an integer number of laser cycles, so we again obtain zero vector potential at the end of the dressing pulse. We assume this field is too weak to excite or ionize the atom on its own, an assumption that we can explicitly check by running the calculation once without the XUV field.

To calculate the cross section for absorption, we begin with the atom in its ground state $|\psi_\mathrm{I}\rangle$ at time t_0 and use the grid-based methods of Ref. [34] to propagate the wave function forward in time until the end of the combined XUV and dressing pulse at time t_f. At this time we calculate the probability that the atom has remained in its ground state $P_\mathrm{I}(t_f)$ by projecting the final wave packet $|\psi(t_f)\rangle$ onto the initial wave packet:

$$P_\mathrm{I}(t_f) = |\langle\psi_\mathrm{I}|\psi(t_f)\rangle|^2. \tag{11}$$

Given $P_I(\infty) = P_I(t_f)$ from the TDSE calculation, we obtain the probability that the atom is excited or ionized from $1 - P_I(t_f)$. Because we are dealing with a one-photon absorption process where we assume the intensity is well below saturation, a linear relation between the XUV absorption rate and XUV photon flux holds: $\Gamma(t) = \sigma(\omega_\mathrm{X})\,J_X(\omega_\mathrm{X},t)$. We use this assumption to transform the probability to absorb an XUV photon into an expression for the cross section:

$$2[1 - P_I(\infty)] = \sigma(\omega_X)\int_{-\infty}^{\infty} J_X(\omega_\mathrm{X},t)\,dt. \tag{12}$$

This is equivalent to the steady-state expression in Eq. (1): The factor 2 again stems from the two electrons in the spatial orbital I that contribute equally.

The underlying assumption in Eq. (12) is that we can calculate the absorption cross section $\sigma(\omega_\mathrm{X})$ for a small range of frequencies $\Delta\omega_\mathrm{X}$ around ω_X by calculating the response of the atom to a pulse of bandwidth $\Delta\omega_\mathrm{X}$. For Eq. (12) to be meaningful, the cross section needs to be approximately constant over the bandwidth $\Delta\omega_X$ of the pulse. For a low-bandwidth pulse, we can further use the relation $I_X(t) \approx \omega_X J_X(\omega_\mathrm{X},t)$ between photon flux and intensity. Then, the time integral on the right-hand side can be solved analytically for the pulse shape (7). In this way, we find the XUV absorption cross sections $\sigma(\omega_\mathrm{X})$ from Eq. (12) by dividing the probability to excite an atom out of the ground state $1 - P_I(t_f)$ by the integral over the XUV flux.

As we stated in the Introduction, though we expect that the two methods for calculating the frequency-dependent absorption cross section should agree, the TDSE projection approach is potentially more flexible in dealing with situations where the dressing laser couples many states of the atom, which forces the Hamiltonian matrix in Eq. (2) to be very large.

C. Time-frequency treatment of ultrafast XUV absorption

In this section we extend the treatment of the XUV interaction to deal with cases where the atomic response varies as a function of time or frequency in a nontrivial way. This could be because the dressing IR pulse is substantially shorter than the XUV pulse, or when nonlinear interactions would cause the atom to exchange energy with multiple XUV frequency components in different nonlinear orders.

We start by deriving a frequency-dependent response function $\widetilde{S}(\omega)$ from the time-dependent energy exchange between the atom and the light field. $\widetilde{S}(\omega)$ is defined so that when integrated over all frequencies, it yields the total excitation probability. This includes excitation to continuum states, i.e., ionization. We can then express the total energy gained by the atom from the light fields, ΔE, as the sum over the frequency-dependent excitation probability $\widetilde{S}(\omega)$ times the photon energy:

$$\Delta E = \int_{-\infty}^{\infty} \omega\, \widetilde{S}(\omega)\, d\omega. \tag{13}$$

To calculate the response function, we use that the total atomic energy gain also can be expressed as a sum over the rate at which energy is gained:

$$\Delta E = \int_{-\infty}^{\infty} \omega\, \widetilde{S}(\omega)\, d\omega = \int_{-\infty}^{\infty} \frac{dE}{dt}\, dt. \tag{14}$$

We calculate this rate directly from our one-electron Hamiltonian, $H = H_A + \mathcal{E}(t)\, z$, as

$$\frac{dE}{dt} = \frac{d}{dt}\langle\psi|H|\psi\rangle = \left\langle\psi\left|\frac{\partial H}{\partial t}\right|\psi\right\rangle = \langle z\rangle\frac{\partial \mathcal{E}}{\partial t}. \tag{15}$$

We note that $\mathcal{E}(t)$ is the full electric field consisting of the sum of the dressing laser and the XUV fields. This means that we are simultaneously treating the exchange of energy between the atom and all frequencies of the light field. In the following we will denote $\langle z\rangle(t)$ by $z(t)$. The time-dependent dipole moment is related to $z(t)$ by $d(t) = -z(t)$ for a single electron. We now calculate ΔE:

$$\Delta E = \int_{-\infty}^{\infty} z(t)\frac{\partial \mathcal{E}}{\partial t}\, dt \tag{16}$$

$$= -\int_{0}^{\infty} \omega\, 2\,\mathrm{Im}[\tilde{z}(\omega)\widetilde{\mathcal{E}}^{*}(\omega)]\, d\omega. \tag{17}$$

In this derivation we have used that both $z(t)$ and $\mathcal{E}(t)$ are real functions of time so that $\tilde{z}(-\omega) = \tilde{z}^{*}(\omega)$ and $\widetilde{\mathcal{E}}(-\omega) = \widetilde{\mathcal{E}}^{*}(\omega)$. Using Eq. (14) we then have an expression for the response function:

$$\widetilde{S}_{+}(\omega) = -2\,\mathrm{Im}[\tilde{z}(\omega)\widetilde{\mathcal{E}}^{*}(\omega)], \quad \omega > 0, \tag{18}$$

where the $+$ subscript on $\widetilde{S}_{+}(\omega)$ explicitly indicates that we are only integrating over positive frequencies.

We calculate the dipole spectrum in the SAE approximation $\tilde{d}_{\mathrm{SAE}}(\omega)$ via the time-dependent acceleration $a(t)$:

$$a(t) = \frac{d^2 z}{dt^2} = -\langle\psi(t)|[H,[H,z]]|\psi(t)\rangle. \tag{19}$$

The dipole spectrum is then given by $\tilde{d}_{\mathrm{SAE}}(\omega) = \tilde{a}(\omega)/\omega^2$, where $\tilde{a}(\omega)$ denotes the Fourier transform of $a(t)$. The full (two-electron) dipole moment is $\tilde{d}(\omega) = 2\tilde{d}_{\mathrm{SAE}}(\omega)$.

In the weak-IR limit, where it is meaningful to talk about an absorption cross section, we can write the frequency-dependent energy-exchange function $\omega\widetilde{S}(\omega)$ by means of a generalized cross section $\tilde{\sigma}(\omega)$ and the spectral energy density of the electric field, $\omega\widetilde{J}(\omega)$. The spectral flux $\widetilde{J}(\omega)$ is defined as [our Fourier transformation convention is $\mathcal{E}(t) = \frac{1}{\sqrt{2\pi}}\int_{-\infty}^{\infty}\widetilde{\mathcal{E}}(\omega)e^{-i\omega t}\, d\omega$ and $\widetilde{\mathcal{E}}(\omega) = \frac{1}{\sqrt{2\pi}}\int_{-\infty}^{\infty}\mathcal{E}(t)e^{i\omega t}\, dt$]

$$\widetilde{J}(\omega) = \frac{1}{4\pi\alpha\omega}|\widetilde{\mathcal{E}}(\omega)|^2, \tag{20}$$

This means that once we calculate the response function $\widetilde{S}(\omega)$, the generalized cross section is given by

$$\tilde{\sigma}(\omega) = \frac{4\pi\alpha\omega\widetilde{S}(\omega)}{|\widetilde{\mathcal{E}}(\omega)|^2}. \tag{21}$$

Inserting the response function from Eq. (18), we obtain the cross section, now defined for both positive- and negative-frequency components,

$$\sigma(\omega) = 8\pi\alpha\omega\,\mathrm{Im}\left[\frac{\tilde{d}_{\mathrm{SAE}}(\omega)}{\widetilde{\mathcal{E}}(\omega)}\right]. \tag{22}$$

This equation is the generalized, time-frequency, multimode equivalent of Eq. (1), which was derived for the steady-state case.

To calculate the generalized cross section in Eq. (22), and the macroscopic polarization field described in the following subsection, we multiply the time-dependent acceleration in Eq. (19) with a window function $W(t)$, $a_W(t) = a(t)W(t)$, and calculate $\tilde{d}_{\mathrm{SAE}}(\omega)$ from the Fourier transform of $a_W(t)$. In Eq. (22) we also calculate $\widetilde{\mathcal{E}}(\omega)$ from $W(t)\mathcal{E}(t)$ for normalization purposes. The window function on the time-dependent acceleration is necessary in particular in those cases where the XUV light is resonant with an atomic transition. The XUV light then induces a strong coherence between the ground state and the excited state, which in the numerical calculation will go on "ringing" until long after the XUV pulse is over. This ringing does not correspond to stimulated emission or absorption of XUV radiation. The window function we use is a trigonometric function as given in Eq. (8), and is in general chosen to have the same FWHM duration as the longer of the IR and XUV pulses. The choice of window function has some influence on the value of the cross section for the undressed atom around the field-free resonances. When the atom is laser dressed so that the XUV light is no longer absorbed as strongly, the ringing is strongly suppressed by the laser field and the influence of the window function is very small.

It is interesting to note here that for intense or few-cycle IR fields, and/or for multimode XUV fields, the sign of the response function $\widetilde{S}_{+}(\omega)$ (and therefore the sign of the generalized cross section) for a particular frequency ω in Eq. (18) can be positive or negative. When $\widetilde{S}_{+}(\omega)$ is positive,

the atom will predominantly absorb light of that frequency, and when $\widetilde{S}_+(\omega)$ is negative, the atom will predominantly emit light of that frequency. This makes the response function a powerful tool for studying the dynamics of the light-atom energy exchange, in particular, in combination with a sliding time window on the time-dependent acceleration. This would in principle allow for the time resolution of when different frequencies are absorbed or emitted during a dynamical process. We will discuss a simple application of this in connection with the macroscopic reshaping of an XUV pulse presented in Sec. V.

III. MACROSCOPIC RESPONSE, INCLUDING ABSORPTION

As we will show at the end of this section, the relationship derived in the previous section, between the dipole spectrum driven by an arbitrary pulse and the absorption cross section for the frequencies contained in that pulse, is consistent with our general framework for the interaction between an ultrafast, multicolor pulse and a macroscopic medium. This framework consists of the coupled solutions of the MWE and the TDSE for all frequencies ω of the electric field $\tilde{E}(\omega)$ of the multicolor pulse. We will express all quantities in SI units in this section. In a frame that moves at the speed of light, and in the slowly evolving wave approximation that works well even for few-femtosecond pulses [38], the MWE takes the following form:

$$\nabla_\perp^2 \tilde{\mathcal{E}}(\omega) + \frac{2i\omega}{c}\frac{\partial \tilde{\mathcal{E}}(\omega)}{\partial z} = -\frac{\omega^2}{\epsilon_0 c^2}[\tilde{P}(\omega) + \tilde{P}_{\rm ion}(\omega)]. \quad (23)$$

The electric field $\tilde{\mathcal{E}}(\omega)$ and the source terms $\tilde{P}(\omega)$ and $\tilde{P}_{\rm ion}(\omega)$ are also functions of the cylindrical coordinates r and z. We solve this equation by space marching through the helium gas, at each plane z in the propagation direction, calculating the response terms $\tilde{P}(\omega)$ and $\tilde{P}_{\rm ion}(\omega)$ via numerical integration of the TDSE, and then using them to propagate to the next plane in z. The macroscopic polarization field $\tilde{P}(\omega)$ is calculated from two times the one-electron single-atom dipole moment $\tilde{d}_{\rm SAE}(\omega)$:

$$\tilde{P}(\omega) = 2\rho\tilde{d}_{\rm SAE}(\omega) = \frac{2\rho e}{\omega^2\sqrt{2\pi}}\int_{-\infty}^{\infty} a(t)W(t)e^{i\omega t}\,dt, \quad (24)$$

where ρ is the atomic density, and $a(t)$ is the time-dependent acceleration calculated as described in Sec. II C. As the driving field for the TDSE calculation, we use the evolving electric field $\mathcal{E}(t)$ at the plane z. This means that $\tilde{P}(\omega)$ in general includes both the linear and nonlinear response of the atom to the multicolor field. The term $\tilde{P}_{\rm ion}(\omega)$ is related to the space- and time-dependent free-electron contribution to the refractive index and is also calculated within the SAE-TDSE (see Ref. [39]). This term is very small in the cases considered in this paper and we will ignore it hereafter.

By calculating the source terms in each z plane and using them to propagate to the next z plane, we are coupling both the linear and nonlinear response generated in one step back into the full electric field so that it can contribute to the driving electric field in the next step. In much of the work described in the literature (see, for instance, Refs. [38–42]), the nonlinear response is separated from the linear response, and the propagation of the newly generated radiation (via nonlinear processes) is separated from the propagation of the driving field. Absorption and dispersion of different frequency components of the light fields are then added separately, typically using tabulated, frequency-dependent values. It has been shown in a number of papers that such an approach offers a very complete description of both the generation of new frequencies via nonlinear processes, and the macroscopic effects of phase matching and ionization-driven reshaping of the ultrafast propagating pulse [38–42]. However, it cannot describe ultrafast or dynamical reshaping of the XUV pulses driven by, for instance, absorption, dispersion, or laser-induced transparency. More generally, processes that are owing to the combined response to the strong dressing or driving laser field and the weaker XUV fields are not described in a self-consistent manner because the generated radiation is not included into the driving field.

In the following we will argue that the approach presented in this paper, which allows us to calculate the nonlinear response of the dressed atom, also allows us to describe the absorption and dispersion of the ultrafast pulses in a self-consistent manner, to within the SAE approximation. Let us first rewrite the macroscopic polarization field as

$$\tilde{P}(\omega) = \rho\tilde{d}(\omega) = \rho\left\{\mathrm{Re}\left[\frac{\tilde{d}(\omega)}{\tilde{\mathcal{E}}(\omega)}\right] + i\,\mathrm{Im}\left[\frac{\tilde{d}(\omega)}{\tilde{\mathcal{E}}(\omega)}\right]\right\}\tilde{\mathcal{E}}(\omega). \quad (25)$$

The last term on the right-hand side is proportional to the generalized cross section in Eq. (22). By inserting this expression into the MWE in Eq. (23) we get

$$\nabla_\perp^2 \tilde{\mathcal{E}}(\omega) + 2i\frac{\partial \tilde{\mathcal{E}}(\omega)}{\partial z} = -\frac{\omega}{\epsilon_0 c}\rho\,\mathrm{Re}\left[\frac{\tilde{d}(\omega)}{\tilde{\mathcal{E}}(\omega)}\right]\tilde{\mathcal{E}}(\omega) - i\rho\tilde{\sigma}(\omega)\tilde{\mathcal{E}}(\omega). \quad (26)$$

The second term on the right-hand side clearly will lead to absorption at frequency ω with absorption coefficient $\rho\tilde{\sigma}(\omega)$ when $\tilde{\sigma}(\omega)$ is positive, which is the case in the weak-field limit when the atomic response is linear. In this linear case, the first term on the right-hand side likewise can be interpreted as a generalized expression for the dispersion experienced in the gas medium, with the frequency-dependent correction to the refractive index given by $\Delta\tilde{n}(\omega) = \frac{\rho}{2\epsilon_0}\mathrm{Re}[\frac{\tilde{d}(\omega)}{\tilde{\mathcal{E}}(\omega)}]$. The strength of our time-dependent approach is that even when the driving field is strong enough to induce nonlinear processes, we are able to treat all of the linear and nonlinear processes within one time-dependent calculation, rather than artificially separating processes of different nonlinearities and assigning them a frequency- and intensity-dependent weight.

IV. COMPUTATIONAL DETAILS

Computations with the time-independent theory of Sec. II A were carried out with the DREYD computer program from the FELLA suite [43]. The computational parameters are specified in analogy to Ref. [19]. However, in this work, we do *not* rely on the Hartree-Fock-Slater mean-field approximation [28,29] to describe the atomic electronic structure. Instead, we use a pseudopotential for helium, constructed from the ground-state Hartree-Fock potential, calculated on a very fine radial grid

by standard iterative methods [44]. We set the K edge of helium to the value of $E_{1s} = -24.5786$ eV. Next, the radial Schrödinger equation is solved with the pseudopotential where the solution, the radial part of the atomic orbitals, is represented on a grid with a radius of $60a_0$ using 3001 finite-element functions. From its eigenfunctions we choose, for each orbital angular momentum l, the 100 functions that are lowest in energy to form atomic orbitals [19]. In doing so, we consider spherical harmonics with up to $l = 7$ [37,45]. Continuum electrons are treated with a smooth exterior complex scaling complex absorbing potential [46–48] which is parametrized with the complex scaling angle $\theta = 0.13$ rad, a smoothness of the path of $\lambda = 5a_0^{-1}$, and an exteriority of $r_0 = 10a_0$ [19]. There is only radiative decay of singly excited states of helium with comparatively long lifetimes to all other time scales in the problem; therefore, we set the linewidth of a K vacancy in helium to zero. Finally, we diagonalize the involved Floquet-type matrices to obtain the cross section. Without the laser field this is done exactly; when the laser is present we use 4000 Lanczos iterations [18].

Computations with the TDSE-projection method of Sec. II B were carried out with a one-electron TDSE solver code that is based on the algorithms described in Ref. [34]. The same potential used above is transferred to a radial grid with a spacing of $0.2a_0$ and used for the TDSE-projection and fully time-dependent computations (see below). The interpolation of the Hartree-Fock potential onto the coarse grid used for the TDSE propagation introduces a small error in the helium $1s$ ionization potential, which we correct by slightly changing the potential at the first grid point [34]. The pulse shape is given by Eqs. (7)–(9) with $n = 6$. This means that the total propagation time is $4.67\tau_X$. Typically we use a box of 200 a.u. in size, with a 50 a.u. absorbing boundary at the outer edge [34]. The maximum angular momentum and time step size are adjusted to achieve convergence. We use $\ell_{\max} = 8$ and 1500 steps per dressing-laser cycle. In some cases where the XUV pulse was very long or the XUV wavelength was very close to the ionization threshold, the box size was increased to 1000 a.u. to ensure that no wave-function amplitude that might reflect from the absorbing boundary could interfere with amplitude excited at a later time. We specify the bandwidth $\Delta\omega_X$ of the XUV pulse instead of the FWHM duration τ_X as in Eq. (8). For our (approximately) Gaussian pulse, we use the time-bandwidth product $\tau_X \Delta\omega_X = 4\ln 2$ to convert between the two quantities [49] with $\Delta\omega_X = 0.05$ eV, which corresponds to a duration of $\tau_X = 36.5$ fs. We investigated the dependence of the absorption cross sections on the intensity of the XUV light; to a very good approximation, we find a linear relationship as should hold for a one-photon absorption process (1). An XUV intensity of 10^{10} W/cm^2 is employed in Figs. 1–4.

The calculations with the time-frequency method of Sec. II C were performed with the TDSE solver described above. For the calculations in Figs. 1(b) and 1(c) and the inset in Fig. 2, we have used $\ell_{\max} = 8$ and ∼4000 steps per cycle of the dressing-laser field. The size of the radial grid was $150a_0$ (using 750 points) with a 250-point absorbing boundary. The intensity envelope of the IR pulse is $\cos^4(\beta t/\tau_{\rm IR})$, where $\tau_{\rm IR}$ is the FWHM duration of the IR pulse and $\beta = 2\arccos(0.5^{1/4})$. The intensity envelope of the XUV is usually chosen to be the fourth power of the IR envelope (to be consistent with the XUV being a high-order harmonic produced by the IR pulse). This gives a FWHM pulse duration for the XUV pulse of approximately half that of the IR pulse. The window function discussed in Sec. II C is a Hann window with a FWHM duration very close to that of the IR pulse. The window function was chosen such that the long-pulse calculations in Fig. 1(b) can be compared to those in Fig. 1(a): The FWHM bandwidth of the windowed acceleration spectrum $\tilde{a}_W(\omega)$ has the same 0.05-eV bandwidth as the TDSE-projection approach.

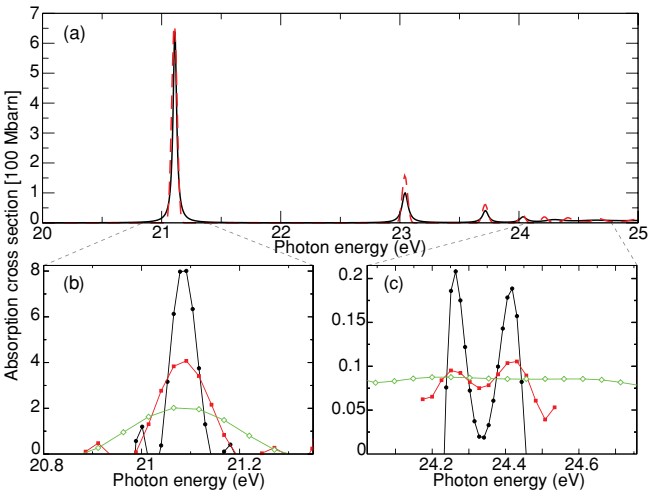

FIG. 1. (Color online) The XUV absorption cross section of a helium atom. (a) The dashed red lines were obtained with DREYD [43] and the solid black lines were obtained using the TDSE-projection method. (b) and (c) show closeups of the cross section around the (b) $2p$ and (c) $6p$ and $7p$ states calculated with the time-frequency method [Eq. (22)] for different XUV pulse durations. The results obtained using 30-, 15-, and 7.5-fs XUV pulses are shown in black (circles), red (squares), and green (open diamonds), respectively.

For the MWE-TDSE calculations in Fig. 6 we employ two time scales. One time scale defines the spectral resolution of the macroscopic, propagating electric fields. This time scale typically extends to $\pm 3\times$ the FWHM of the longest of the IR and XUV pulses and contains ∼5500 time points. The other

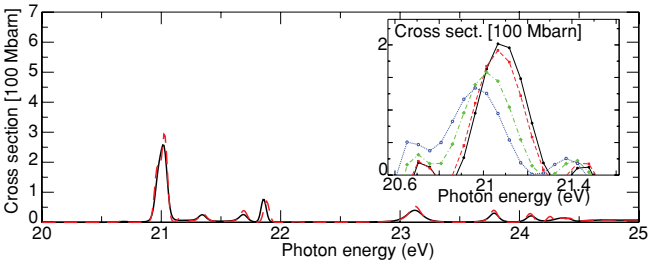

FIG. 2. (Color online) The XUV absorption cross section of a helium atom dressed by an intense 800-nm IR laser pulse with a peak intensity of 10^{12} W/cm^2. The dashed red lines were obtained with DREYD [43]; the cross section obtained from the TDSE projection is plotted with dashed black lines. The inset shows the cross section calculated using Eq. (22), using an XUV pulse duration of 7.5 fs, and a 764-nm IR pulse with a duration of 15 fs and a peak intensity of 10^8 W/cm^2 (solid black curve), 10^{11} W/cm^2 (dashed red curve), 5×10^{11} W/cm^2 (dotted-dashed green curves), or 10^{12} W/cm^2 (dotted blue curve), respectively.

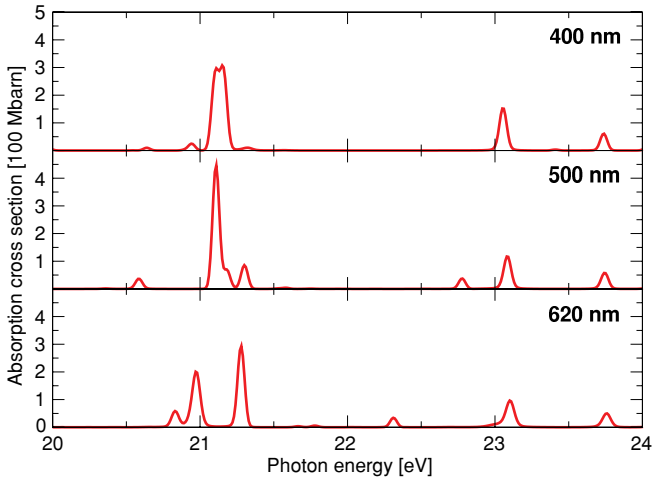

FIG. 3. (Color online) Laser-dressed XUV absorption cross section of helium for 400-, 500-, and 620-nm laser wavelengths at a laser intensity of 10^{12} W/cm^2.

time scale is used for the TDSE solution and extends only over the finite duration of the longest pulse, and typically contains 6000 points per IR laser cycle. The macroscopic length scales cover 160 μm in the radial direction, with 200 grid points, 40 of which contain an absorber that prevents reflections from the edge of the grid, and 1 mm in the propagation direction, with 600 grid points. In the propagation direction we only evaluate the dipole moment every 20 steps, and rescale the response to the appropriate density and phase in between (see Ref. [39] for details). The initial spatial distribution of both the XUV and the dressing-laser beam is Gaussian. The XUV beam has a confocal parameter of 10 cm and a corresponding focal diameter of 60 μm. The 1600-nm dressing pulse has a confocal parameter of 2 cm and a focal diameter of 140 μm. This means that in the spatial dimension, the XUV beam is always overlapped with the IR beam. The IR beam changes only marginally during the propagation in the helium gas.

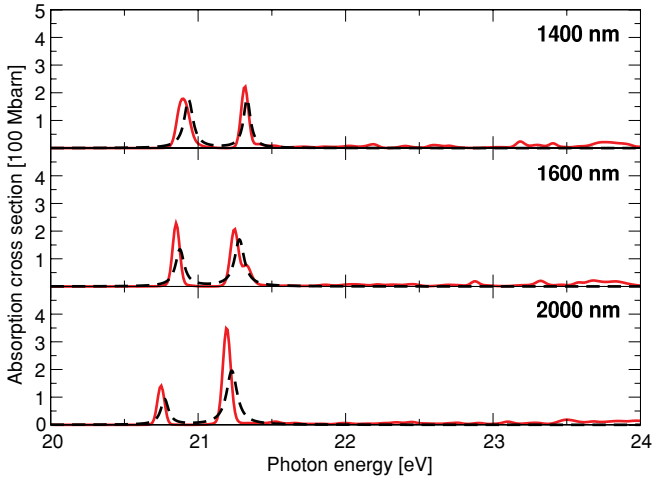

FIG. 4. (Color online) Laser-dressed XUV absorption cross section of helium for 1400-, 1600-, and 2000-nm laser wavelengths at a laser intensity of 10^{12} W/cm^2 (red solid curves). The results of the simple three-level model of Fig. 5 are indicated by the dashed black curves for $\Gamma_{1s^{-1}2p} = 0.1$ eV and $\Gamma_{1s^{-1}2s} = 0.05$ eV.

V. RESULTS AND DISCUSSION

A. Single-atom absorption cross sections

The helium absorption cross section for linearly polarized XUV light, in the absence of laser light, is displayed in Fig. 1. In Fig. 1(a), we compare results from DREYD [43] with results of the TDSE-projection method [Eq. (12)]. To be able to compare these two results, we have convoluted the DREYD cross sections with a Gaussian with the same bandwidth of $\Delta\omega_X = 0.05$ eV that was used in the TDSE calculation. This leads to good agreement between the two results. We note that the presence of a spectral bandwidth in both calculations means that we are only able to resolve spectral features to within 0.05 eV. The peaks at 21.1068 eV, 23.0416 eV, 23.7162 eV, 24.0273 eV, . . . stem from $1s^2 \rightarrow 1snp$ transitions with $n \in \{2,3,4,5,\ldots\}$. In Figs. 1(b) and 1(c) we show cross sections calculated using the time-frequency approach leading to Eq. (22), around the $2p$ and the $6p$ and $7p$ states. These calculations were done using an extremely weak 764-nm IR pulse and harmonics 13 [Fig. 1(b)] or 15 [Fig. 1(c)] of the IR frequency (the IR field is included as a technical convenience for performing the low-IR intensity and high-IR intensity calculations consistently, both for the time-frequency approach and for the MWE-TDSE approach). Harmonic 13 is resonant with the $2p$ state and harmonic 15 is in between the $6p$ and the $7p$ states. We show the results of using three different XUV pulse durations (30, 15, and 7.5 fs). The IR pulse has twice the duration of the XUV pulse and an intensity of 10^8 W/cm^2 (low enough that it does not influence the cross sections). The 30-fs calculation leads to a 0.05-eV bandwidth of the dipole moment around the $2p$ state, after applying the time-domain window function discussed in Sec. IV. The calculated cross section is in reasonably good agreement with the results in Fig. 1(a). The shorter XUV pulses lead to broader absorption cross sections. For the 15-fs XUV pulse the $6p$ and $7p$ states still can be distinguished as separate features in the absorption spectrum. Using a 7.5-fs XUV pulse, the cross section can be calculated over a much larger frequency range, spanning both below and above the ionization threshold, and as a consequence one can no longer distinguish the $6p$ and $7p$ states. The value of the cross section in this calculation is in good agreement with the value in Henke *et al.* [50] of 7.5 Mb just above threshold, as we expect when using pulses that span the ionization threshold.

In Fig. 2 we show how the XUV cross section changes when the helium atom is exposed to an infrared laser field with an intensity of 10^{12} W/cm^2 and a wavelength of $\sim$800 nm. The main figure again compares the results from DREYD [43] and the TDSE-projection method (which have again both been calculated or convoluted with a 0.05-eV bandwidth), and they are found to be in good agreement over a broad energy range.

The absorption of the dressed atom in Fig. 2 changes significantly from the undressed case, although many of the field-free resonances still can be recognized. The peak owing to the $2p$ state has broadened and shifted to lower energy, whereas the higher np peaks are shifted to higher energies. In addition, several new absorbing features have appeared between 21 and 22 eV. The inset in Fig. 2 shows cross sections for the dressed helium atom calculated using the time-frequency approach of Eq. (22), for an XUV pulse duration of 7.5 fs. The 764-nm IR pulse duration is 15 fs and the IR peak intensity varies

TABLE I. Correspondence between wavelength and photon energy for the involved laser light.

Wavelength (nm)	400	500	620	800	1400	1600	2000
Photon energy (eV)	3.10	2.48	2.00	1.55	0.89	0.78	0.62

between 10^8 W/cm^2 [undressed, as shown in Fig. 1(b)] and 10^{12} W/cm^2. The inset details the shift and broadening of the $2p$ resonance as the dressing-laser intensity is increased. We have chosen to use the 7.5-fs XUV pulses for these calculations in order to be able to cover the shift of the $2p$ resonance within the bandwidth that can be addressed within Eq. (22).

The extra peaks in the 800-nm dressed-atom cross section shown in Fig. 2 result from complex multiphoton effects and do not have a straightforward interpretation. Other dressing-laser wavelengths offer more insight into the nonlinear optics driven by the two-color field. We first show two figures exploring the impact of the dressing-laser wavelength on the XUV absorption cross section. The wavelengths we have used are listed in Table I, together with the corresponding photon energies. All of these wavelengths can be produced from standard Ti:sapphire high-power, short-pulse laser systems via frequency mixing in nonlinear materials.

The laser-dressed XUV absorption cross section, calculated using the TDSE-projection method, are displayed in Figs. 2–4 for several laser wavelengths at an intensity of 10^{12} W/cm^2. For 400- and 500-nm light, we see only a moderate impact of the laser dressing. The impact is mostly on the $2p$ state, as the largest dipole coupling exists to other close-by Rydberg states. The 620- and 800-nm light exhibit complex multiphoton effects that manifest in complicated multipeak structures in the cross sections. The dressing pulses with longer wavelengths all induce systematic behavior. In all three cases, the single $1s^2 \rightarrow 1s2p$ transition in Fig. 1(a) (without dressing) is split into two lines by the laser in Fig. 3; the transitions from the $1s$ orbital into higher Rydberg orbitals are replaced by a continuous, weak absorption feature.

We would like to elucidate the origin of the double-peak feature centered around 21 eV in the long-wavelength series shown in Fig. 4. It is much simpler than the corresponding feature for the wavelengths in Figs. 2 and 3. To this end, we make a Λ-type model for helium that is shown in Fig. 5. It comprises the ground state of helium and the $1s^{-1}2p$ and $1s^{-1}2s$ excited states. The laser photon energy is denoted by ω_L whereas $\Gamma_{1s^{-1}2s}$ and $\Gamma_{1s^{-1}2p}$ are parameters for the laser-induced decay widths of the respective excited states. The overall agreement of the model curves with the *ab initio* data in Fig. 4 is satisfactory. The reason for the success of the three-level model is—as in Ref. [7]—the fact that the splitting between the $2s$ and $2p$ Rydberg orbitals in helium is 0.84 eV, i.e., the laser is almost in resonance with this transition, within the laser-induced linewidths, for midinfrared wavelengths (Table I). Furthermore, the other levels of helium couple only weakly.

The Λ-type model explains the double-peaked structure in Fig. 4 in terms of a splitting of the $1s^{-1}2p$ and $1s^{-1}2s$ states into an Autler-Townes doublet. This feature raises the possibility that the dressing laser could be used to induce

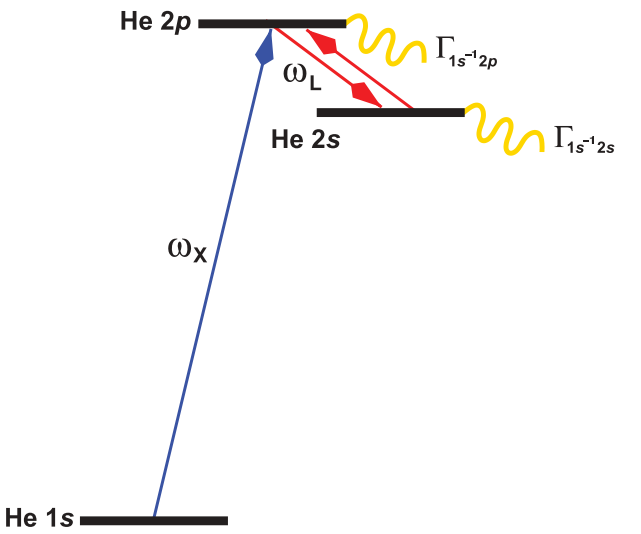

FIG. 5. (Color online) Λ-type three-level model for helium. The laser photon energy is ω_L and the XUV photon energy is ω_X. The laser-induced decay widths of the $1s^{-1}2p$ and $1s^{-1}2s$ excited states are denoted by $\Gamma_{1s^{-1}2p}$ and $\Gamma_{1s^{-1}2s}$, respectively.

transparency to the XUV radiation tuned to the $1s^2 \rightarrow 1s2p$ transition. A similar mechanism was found for the suppression of resonant absorption of x rays in neon [7,15–17], argon [18], and krypton [19] atoms and called EIT for x rays [7]. In the next section we study the analogous effect in helium.

B. XUV pulse shaping in a macroscopic medium

In this section we present an application of the time-frequency approach to absorption in a macroscopic nonlinear medium. We study how the laser-induced transparency discussed above may be used to temporally control the XUV pulse shape in a helium gas, in analogy with the EIT for x rays discussed in Ref. [18]. In that x-ray study, the absorption was exclusively described in terms of an intensity-dependent absorption cross section, which then in turn enforces a one-to-one mapping of the absorption to time through the intensity. This does not allow for truly dynamical effects. In addition, the intensities we explore here are much lower that those used in the x-ray study, which means that ionization of the Rydberg states does not play a large role.

We calculate the electric field of a combined two-color XUV-IR pulse after propagation through a 1-mm-long helium gas jet with a density of 1.5×10^{17} cm^{-3} (6 mbar at room temperature). We solve the coupled MWE-TDSE in the form of Eq. (23) as described in Sec. III (see also Ref. [39]). The initial XUV pulse has a wavelength of 58.7 nm (21.1 eV, resonant with the $1s^2 \rightarrow 1s2p$ transition), a pulse duration of 61 fs, and a peak intensity of 10^7 W/cm^2. The 1600-nm dressing pulse has a peak intensity of 10^{12} W/cm^2. We have used different IR pulse durations between 122 and 11 fs. We have checked that the reshaping discussed below is no different when we use a higher XUV intensity of 10^{10} W/cm^2.

Figure 6 shows (a) the radially integrated spectrum and (b) time profile of the XUV pulse before and after propagation through the helium gas. When the atoms are undressed, the XUV radiation is strongly depleted via the resonant absorption,

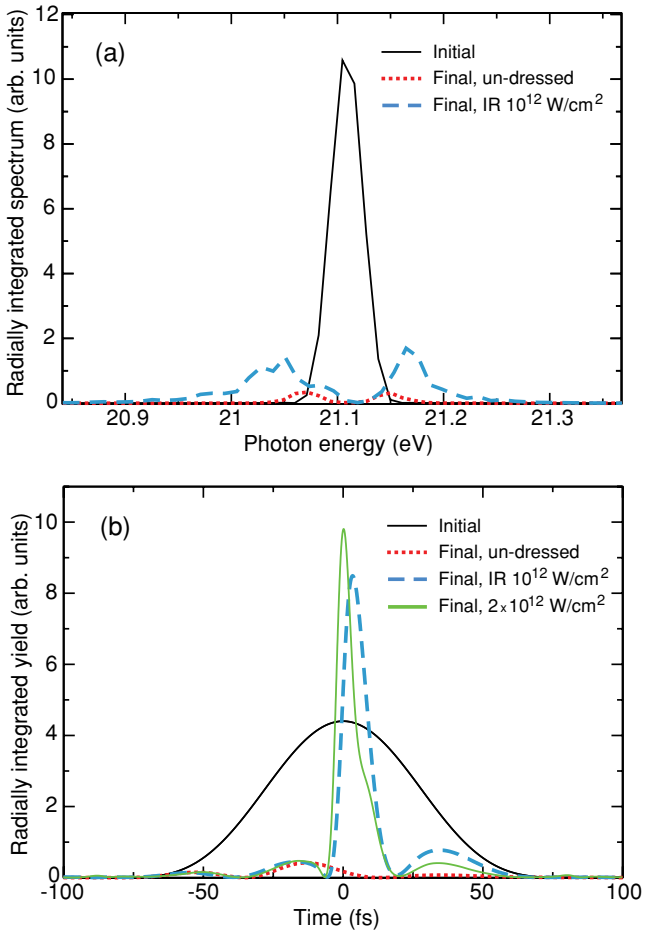

FIG. 6. (Color online) IR-assisted XUV absorption in 1-mm-long macroscopic helium gas with a density of 4×10^{16} cm^{-3}. The initial 61-fs XUV pulse is resonant with the $2p$ state of the undressed helium atom. We show the XUV spectrum in (a) and time profile in (b), both before (solid lines) and after propagation. Final profiles at the end of the undressed medium are shown as dotted red lines, and final profiles at the end of the medium dressed by an 11-fs, 1600-nm IR pulse with a peak intensity of 10^{12} W/cm^2 are shown as dashed blue lines. In (b) we also show the final time profile when the intensity of the dressing pulse is 2×10^{12} W/cm^2 (thin green line).

as is shown by the dotted red lines (we note that a weak 61-fs IR pulse with a peak intensity of 10^8 W/cm^2 was present in this calculation for computational consistency with the dressed-field calculation; we have checked that the presence of this pulse does not alter the results). The absorption length at this atomic density is less than 0.1 mm. During the first few absorption lengths, the XUV yield decreases exponentially. The large dispersion across the resonance, and to a lesser extent the frequency dependence of the absorption cross section, subsequently leads to reshaping of the depleted beam upon further propagation in the gas. This causes the double-peaked shape of the spectrum emerging at the end of the medium. The time profile of the final XUV field is correspondingly irregular, as seen by the red dotted line in Fig. 6(b).

We then apply a 1600 nm, 10^{12} W/cm^2 dressing pulse that is much longer than the XUV pulse (123 fs versus 61 fs). This means that the XUV pulse encounters a sample of strongly dressed atoms that are no longer resonant with the XUV energy (see Fig. 4), and the gas is therefore transparent to the XUV light. The spectrum of the final XUV pulse is nearly indistinguishable from the initial spectrum and is not shown in Fig. 6(a). The final XUV pulse shape is also nearly identical to the initial pulse shape except for a 1.6-fs delay caused by the different group velocities of the IR and the XUV pulses (also not shown in the figure).

Next, we apply an 11-fs dressing IR pulse that is substantially shorter than the XUV pulse. This means that the dressing pulse turns on and off within the FWHM duration of the XUV pulse, thereby strongly coupling the $2s$ and $2p$ states in a dynamical manner. The final spectral and temporal XUV profiles at the end of the medium are shown with dashed blue lines in Figs. 6(a) and 6(b). The XUV time profile at the end of the medium is dominated by an $\sim$10 fs pulse, superimposed on a much weaker longer pulse, and the corresponding XUV spectrum has broad shoulders at frequencies substantially beyond the initial XUV bandwidth. We note that the final XUV pulse is not symmetric around time zero and that, in particular, the short subpulse is delayed by $\sim$4 fs from the center of the dressing IR pulse. We attribute this to the complicated absorption and emission dynamics driven by the two-color pulse, as explored in more detail next.

The time-dependent acceleration driven by the initial two-color pulse is shown in Fig. 7 (solid black line). We are showing the envelope of the acceleration to avoid the fast oscillations at the resonance frequency. On the rising edge of the XUV pulse, before the IR pulse turns on, this acceleration represents the absorption of the XUV light via population transfer to the $2p$ state. This means that when the IR pulse arrives there is already population in the $2p$ state that will couple strongly to the $2s$ state. This causes the suppression of the acceleration, which starts at approximately $t = -5$ fs. The acceleration then has a revival around 4 fs before it is suppressed again. By calculating the generalized cross sections of Eq. (22) separately for the peaks around $t = -9$ fs and around $t = +4$ fs, we find that they have opposite signs. This means that whereas the dipole

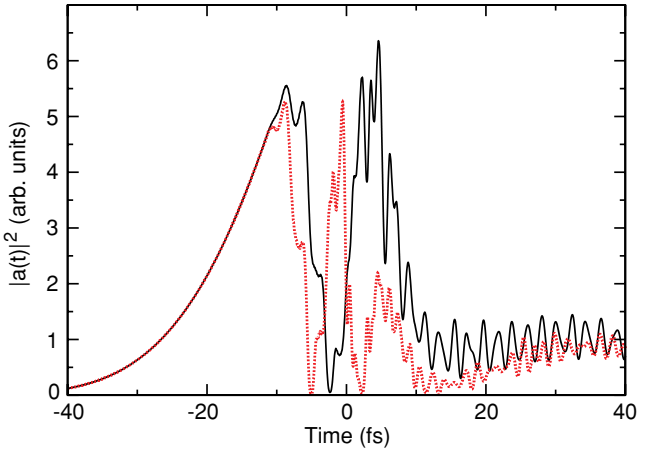

FIG. 7. (Color online) Single-atom time-dependent acceleration driven by the initial XUV-IR pulse in Fig. 6. The durations of the two pulses are 61 and 11 fs, respectively, and the XUV intensity is 10^7 W/cm^2. The result of using an IR intensity of 1×10^{12} W/cm^2 is shown as a solid black line, and as a dotted red line when the IR intensity is 3×10^{12} W/cm^2.

response early in the pulse and up until $t \approx -5$ fs is owing to the absorption of the XUV light, the peak in Fig. 7 around $t = +4$ fs corresponds to *emission* of XUV radiation. We interpret this behavior as coming from Rabi-like oscillations of the excited-state population between the $2s$ and the $2p$ states, driven by the IR field. The emission happens when the population returns to the $2p$ state while the strong IR field is still on. This interpretation would predict that at higher IR intensity the Rabi cycling should be faster. Indeed, we find that if we increase the IR intensity to 3×10^{12} W/cm^2, the time-dependent acceleration has two revivals within the IR pulse duration, both corresponding to emission (dashed red line in Fig. 7). The Rabi oscillation period for resonant population transfer between the $2s$ and the $2p$ states is $\sim$10 fs (6 fs) for a constant intensity of 1×10^{12} W/cm^2 (3×10^{12} W/cm^2). This is in good agreement with the time scale of the oscillations in the acceleration seen in Fig. 7, especially considering that the IR intensity is changing rapidly between $t = -10$ fs and $t = 10$ fs.

Finally, returning to Fig. 6(b) and the XUV pulse that emerges from the helium gas dressed by the 11-fs IR pulse, we can now attribute the delay of the short XUV pulse to the excited-state dynamics in the strongly dressed atomic gas. Figure 8 shows the evolution of the XUV time profile shown in Fig. 6 as a function of propagation distance. The complicated atomic response shown in Fig. 7, which includes

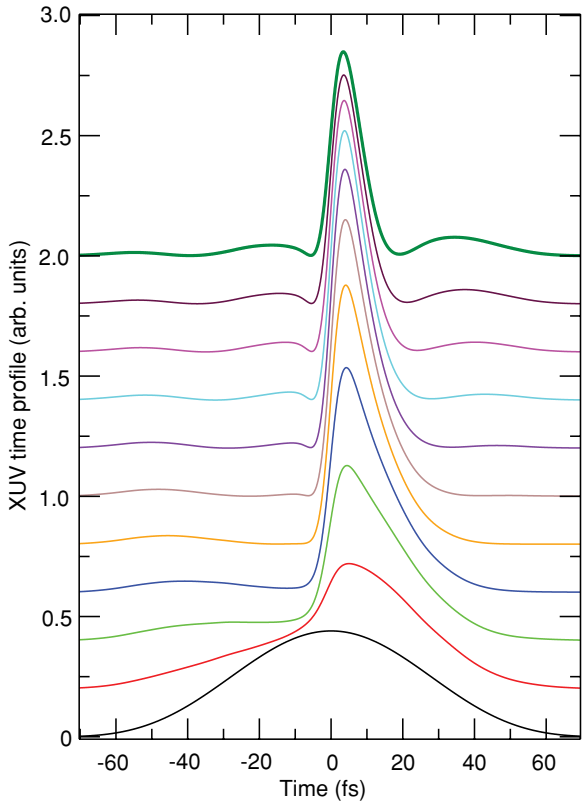

FIG. 8. (Color online) Evolution of XUV time profile during propagation through the macroscopic helium gas. The time profiles at different propagation distances have been displaced vertically, starting with $z = 0$ at the bottom to $z = 1.0$ mm at the top, in increments of $\Delta z = 0.01$ mm.

absorption at early times and emission at approximately $t = 4$ fs, is reflected in the propagating XUV electric field. After the first few hundred micrometers of propagation, the XUV time profile has been substantially depleted on the rising edge, and is dominated by a much shorter pulse peaking shortly after $t = 0$. We note that this in turn will change the atomic response from that plotted in Fig. 7 because the dressing IR pulse and the XUV pulse are then more comparable in duration.

VI. CONCLUSION

In this paper, we have investigated the response of laser-dressed helium atoms to XUV radiation, within the SAE approximation. In particular, we have focused on the calculation of absorption cross sections and their application to absorption in a macroscopic medium.

First, we introduced a time-independent method based on NHPT. The interaction with the XUV light was treated in terms of a one-photon process while a Floquet-like approximation was used to describe the impact of the dressing laser. Second, we devised a time-dependent method to compute the cross section by using a direct integration of the TDSE and projection of the final wave packet onto the initial atomic state. We showed that the projection-based approach, which was implemented using finite pulses, yields the same results compared with the time-independent results. Third, we presented a versatile time-frequency approach to evaluating an atomic response function that can be used even when the dressing-laser pulse is so short that it introduces transient effects, or in cases where the atom exchanges energy with multiple frequency components of the multicolor light field. We showed that this method, when used to calculate linear absorption cross sections, agrees with the first two. Finally, we showed that this third approach can be implemented in a combined MWE-TDSE solver to describe absorption and ultrafast pulse reshaping in a macroscopic medium.

We used the TSDE-projection method to investigate the dependence of the XUV absorption cross section on the wavelength of the laser dressing at 10^{12} W/cm^2 laser intensity. We found complex multiphoton physics for 800-nm light and shorter wavelengths. For longer, midinfrared wavelengths, however, we showed that the impact of the laser dressing on the $1s \rightarrow 2p$ transition in helium can be described in terms of a Λ-type three-level model previously used to describe EIT for x rays [7]. As in the earlier study, the transparency in helium is caused predominantly by Autler-Townes splitting brought about by the strong one-photon coupling induced by the dressing laser, in this case between the $2p$ and $2s$ states. We investigated the macroscopic reshaping of an ultrafast XUV pulse resonant with this transition, for the case when the transparency is induced by an IR pulse that is substantially shorter than the XUV pulse. This means that the absorption properties of the helium atom change dynamically during its interaction with the XUV light. We found rich temporal reshaping dynamics in which the atoms both absorb and subsequently emit the XUV radiation in a process strongly influenced by Rabi oscillations between the $2s$ and $2p$ states. This leads to an XUV pulse emerging from the macroscopic medium that has been shortened from 60 to 10 fs and whose peak intensity has increased by approximately a factor of 2.

The increase in the peak intensity, which results from the coherent population pumped into the $2p$ state before the dressing pulse arrives, is a truly dynamical effect that cannot be described in terms of a single absorption cross section only.

Our results open up several possibilities for future research on ultrafast quantum optics. The control of XUV absorption by laser dressing of helium enables, for example, the possibility for postgeneration ultrafast shaping of XUV pulses [7]. And although we have confined ourselves in this work to the case of one XUV field with a dressing laser, it is a straightforward extension of the method to treat multiple XUV frequencies, some of which could be resonant with dressed atomic transitions, and the complex interferences that would result from this [1,3]. Also, we have used moderately strong IR fields that do not cause any excitation on their own, but the time-dependent treatment is not limited to these intensities. Using higher IR intensities will lead to generation of harmonics in the nonlinear medium. Harmonics with energies below and slightly above the ionization threshold, for which absorption dynamics plays the largest role, have recently attracted much attention, for instance, as a source of vuv and XUV frequency combs [51] or as a seed for free-electron lasers [52]. The treatment of these processes necessitates using methods we have developed in this paper, because the atomic absorption and emission properties will be changing on an ultrafast time scale.

ACKNOWLEDGMENTS

This work was supported by the National Science Foundation under Grant No. PHY-0449235 (C.B. and J.T.), No. PHY-0701372 (K.S.), and No. PHY-1019071 (M.G.). We also acknowledge support from the PULSE Institute at Stanford University (M.G. and K.S.) and from the Marie Curie International Reintegration Grant (C.B.) within the 7th European Community Framework Program (call identifier: FP7-PEOPLE-2010-RG, proposal No. 266551). High-performance computational resources were provided by the Louisiana Optical Network Initiative, www.loni.org.

[1] P. Johnsson, J. Mauritsson, T. Remetter, A. L'Huillier, and K. J. Schafer, Phys. Rev. Lett. **99**, 233001 (2007).
[2] T. E. Glover *et al.*, Nat. Phys. **6**, 69 (2009).
[3] P. Ranitovic *et al.*, New J. Phys. **12**, 013008 (2010).
[4] E. Goulielmakis *et al.*, Nature (London) **466**, 739 (2010).
[5] J. Mauritsson *et al.*, Phys. Rev. Lett. **105**, 053001 (2010).
[6] M. Wickenhauser, J. Burgdörfer, F. Krausz, and M. Drescher, Phys. Rev. Lett. **94**, 023002 (2005).
[7] C. Buth, R. Santra, and L. Young, Phys. Rev. Lett. **98**, 253001 (2007).
[8] T. Pfeifer, M. J. Abel, P. M. Nagel, A. Jullien, Z.-H. Loh, M. J. Bell, D. M. Neumark, and S. R. Leone, Chem. Phys. Lett. **463**, 11 (2008).
[9] M. Drescher, M. Hentschel, R. Kienberger, M. Uiberacker, V. S. Yakovlev, A. Scrinzi, T. Westerwalbesloh, U. Kleineberg, U. Heinzmann, and F. Krausz, Nature (London) **419**, 803 (2002).
[10] T. Remetter *et al.*, Nat. Phys. **2**, 323 (2006).
[11] K.-J. Boller, A. Imamoglu, and S. E. Harris, Phys. Rev. Lett. **66**, 2593 (1991).
[12] M. Fleischhauer, A. Imamoglu, and J. P. Marangos, Rev. Mod. Phys. **77**, 633 (2005).
[13] C. Buth and K. J. Schafer, Phys. Rev. A **80**, 033410 (2009).
[14] M. Swoboda, T. Fordell, K. Klünder, J. M. Dahlström, M. Miranda, C. Buth, K. J. Schafer, J. Mauritsson, A. L'Huillier, and M. Gisselbrecht, Phys. Rev. Lett. **104**, 103003 (2010).
[15] R. Santra, C. Buth, E. R. Peterson, R. W. Dunford, E. P. Kanter, B. Krässig, S. H. Southworth, and L. Young, J. Phys.: Conf. Ser. **88**, 012052 (2007).
[16] C. Buth, R. Santra, and L. Young, Rev. Mex. Fis. S **56**, 59 (2010).
[17] L. Young, C. Buth, R. W. Dunford, P. J. Ho, E. P. Kanter, B. Krässig, E. R. Peterson, N. Rohringer, R. Santra, and S. H. Southworth, Rev. Mex. Fis. S **56**, 11 (2010).
[18] C. Buth and R. Santra, Phys. Rev. A **78**, 043409 (2008).
[19] C. Buth and R. Santra, Phys. Rev. A **75**, 033412 (2007).
[20] T. Laarmann, A. R. B. de Castro, P. Gürtler, W. Laasch, J. Schulz, H. Wabnitz, and T. Möller, Phys. Rev. A **72**, 023409 (2005).
[21] D. Charalambidis, P. Tzallas, N. A. Papadogiannis, L. A. A. Nikolopoulos, E. P. Benis, and G. D. Tsakiris, Phys. Rev. A **74**, 037401 (2006).
[22] T. Laarmann, A. R. B. de Castro, P. Gürtler, W. Laasch, J. Schulz, H. Wabnitz, and T. Möller, Phys. Rev. A **74**, 037402 (2006).
[23] E. Cormier and P. Lambropoulos, J. Phys. B **30**, 3095 (1997).
[24] D. J. Tannor, *Introduction to Quantum Mechanics: A Time-Dependent Perspective* (University Science Books, Sausalito, CA, 2007).
[25] W. T. Pollard and M. R. A., Annu. Rev. Phys. Chem. **43**, 497 (1992).
[26] A. Szabo and N. S. Ostlund, *Modern Quantum Chemistry: Introduction to Advanced Electronic Structure Theory*, 1st revised ed. (McGraw-Hill, New York, 1989).
[27] C. Buth, R. Santra, and L. S. Cederbaum, Phys. Rev. A **69**, 032505 (2004).
[28] J. C. Slater, Phys. Rev. **81**, 385 (1951).
[29] J. C. Slater and K. H. Johnson, Phys. Rev. B **5**, 844 (1972).
[30] V. I. Kukulin, V. M. Krasnopol'sky, and J. Horáček, *Theory of Resonances* (Kluwer, Dordrecht, 1989).
[31] N. Moiseyev, Phys. Rep. **302**, 211 (1998).
[32] R. Santra and L. S. Cederbaum, Phys. Rep. **368**, 1 (2002).
[33] A. J. F. Siegert, Phys. Rev. **56**, 750 (1939).
[34] K. J. Schafer, in *Strong Field Laser Physics*, edited by T. Brabec, Springer Series in Optical Sciences, Vol. 134 (Springer, New York, 2008), pp. 111–145.
[35] D. P. Craig and T. Thirunamachandran, *Molecular Quantum Electrodynamics* (Academic, London, 1984).
[36] I. Barth and C. Lasser, J. Phys. B **42**, 235101 (2009).
[37] G. B. Arfken and H. J. Weber, *Mathematical Methods for Physicists*, 6th ed. (Elsevier Academic, New York, 2005).
[38] T. Brabec and F. Krausz, Rev. Mod. Phys. **72**, 545 (2000).

[39] M. B. Gaarde, J. L. Tate, and K. J. Schafer, J. Phys. B **41**, 132001 (2008).
[40] A. L'Huillier, P. Balcou, S. Candel, K. J. Schafer, and K. C. Kulander, Phys. Rev. A **46**, 2778 (1992).
[41] E. Priori *et al.*, Phys. Rev. A **61**, 063801 (2000).
[42] V. S. Yakovlev, M. Y. Ivanov, and F. Krausz, Opt. Express **15**, 15351 (2007).
[43] C. Buth and R. Santra, FELLA—*the Free Electron Laser Atomic, Molecular, and Optical Physics Program Package, Argonne National Laboratory, Argonne, IL, USA* (2008), version 1.3.0, with contributions by Mark Baertschy, Kevin Christ, Chris H. Greene, Hans-Dieter Meyer, and Thomas Sommerfeld, [http://www.cse.anl.gov/Fundamental_Interactions/AMO_FELLA.html] [www.cse.anl.gov/Fundamental_Interactions/AMO_FELLA.html].
[44] S. E. Koonin, *Computational Physics* (Westview, Boulder, CO, 1998).
[45] E. Merzbacher, *Quantum Mechanics*, 3rd ed. (Wiley, New York, 1998).
[46] N. Moiseyev, J. Phys. B **31**, 1431 (1998).
[47] U. V. Riss and H.-D. Meyer, J. Phys. B **31**, 2279 (1998).
[48] H. O. Karlsson, J. Chem. Phys. **109**, 9366 (1998).
[49] J.-C. Diels and W. Rudolph, *Ultrashort Laser Pulse Phenomena*, 2nd ed. (Academic, Amsterdam, 2006).
[50] B. Henke, E. Gullikson, and J. Davis, At. Data Nucl. Data Tables **54**, 181 (1993).
[51] D. C. Yost, T. R. Schibli, J. Ye, J. L. Tate, J. Hostetter, M. B. Gaarde, and K. J. Schafer, Nat. Phys. **5**, 815 (2009).
[52] X. He *et al.*, Phys. Rev. A **79**, 063829 (2009).